Fluidization Enhancement of Agglomerates of Metal Oxide Nanopowders by Microjets

Jose A. Quevedo, Ayokunle Omosebi, and Robert Pfeffer
Otto York Dept. of Chemical, Biological, and Pharmaceutical Engineering,
New Jersey Institute of Technology, Newark, NJ 07102

DOI 10.1002/aic.12075
Published online October 29, 2009 in Wiley InterScience (www.interscience.wiley.com).

The quality of gas–solid fluidization of agglomerates of nanoparticles has been greatly enhanced by adding a secondary flow in the form of a high-velocity jet produced by one or more micronozzles pointing vertically downward toward the distributor. The micronozzles produced a jet with sufficient velocity (hundreds of meters per second), turbulence, and shear to break-up large nanoagglomerates, prevent channeling, curtail bubbling, and promote liquid-like fluidization. For example, Aerosil R974, an agglomerate particulate fluidization (APF) type nanopowder, expanded up to 50 times its original bed height, and difficult to fluidize agglomerate bubbling fluidization (ABF) type nanopowders, such as Aeroxide TiO2 P25, were converted to APF type behavior, showing large bed expansions and homogeneous fluidization without bubbles. Microjet-assisted nanofluidization was also found to improve solids motion and prevent powder packing in an internal, is easily scaled-up, and can mix and blend different species of nanoparticles on the nanoscale. © 2009 American Institute of Chemical Engineers *AIChE J,* 56: 1456–1468, 2010
Keywords: fluidization, nanoagglomerates, nanopowder, microjet, nozzle, turbulence

Introduction

The study of the hydrodynamic behavior of amorphous nanosize particles in gas–solid fluidized beds has been the focus of extensive research recently due to the increased importance of using nanosize particles to develop advanced composite materials having desirable properties that differ quite significantly from those of bulk materials. Gas–solid fluidization is extensively used in industry for dispersing particulates in a gas phase for different purposes such as gas-solid reactions, modifying powder properties by coating or granulation, adsorption and desorption, blending and mixing, and drying, among others. It is highly probable that nanosize particles will be incorporated as part of large scale industrial processes in the near future, requiring large amounts of nanosize particles to be handled and processed, in many cases using fluidization as the unit operation.

Correspondence concerning this article should be addressed to R. Pfeffer at this current address: Dept. of Chemical Engineering, Arizona State University, Tempe, AZ 85287; e-mail: robert.pfeffer@asu.edu
Current Address of J. A. Quevedo: Shell Global Solutions, P.O. Box 38000, 1030BN Amsterdam, The Netherlands

Nanoparticles cannot be fluidized as individual particles but instead fluidize in the form of large (100–400 μm), highly porous (internal porosity greater than 98%), hierarchical fractal structured agglomerates. Also, the hydrodynamic characteristics and fluidization behavior of nanopowders are quite different from any of the powders classified under the Geldart criteria.[1] Many nanopowders form large agglomerates simply due to storage and are very difficult to fluidize because of the large cohesive forces between the particles, given their size and extensive surface area. When fluidized at high superficial velocity, vigorous bubbling is observed with significant elutriation. Hence, the objective of this research was to develop a new, effective, and simple method that can be used to improve the fluidization quality of nanopowders for industrial applications.

Previous work on the fluidization of nanopowders

Wang et al.[2] studied the fluidization of various fumed silica nanoparticles showing that hydrophobic nanoparticles expanded several times, from 2.5 up to 10 times their initial bed height and that hydrophilic nanoparticles expanded only

1.5 up to three times their initial bed height. They also found relatively large minimum fluidization velocities for the hydrophilic nanoparticles. In their article, they introduced the classification of the fluidization of nanopowders into ''agglomerate particulate fluidization'' (APF) and ''agglomerate bubbling fluidization'' (ABF) to distinguish between smooth, liquid-like, bubble-less fluidization and bubbling fluidization with very little bed expansion

Zhu et al.[3] used a force field generated by sound to enhance the fluidization of APF type Aerosil R974 fumed silica nanoparticles. At frequencies of 50 or 100 Hz, they obtained a larger bed expansion and also a reduction in the minimum fluidization velocity due to the sound waves, which were generated by a loudspeaker located at the top of the bed. However, at frequencies greater than 200 Hz, they observed large bubbles which do not occur with aeration alone. More recently, Guo et al.[4] studied acoustically enhanced fluidized beds of 0.5 μm size titania and silica particles. Guo et al.[5] also fluidized fumed silica nanoparticles under the influence of an acoustic field, and at low frequencies less than 200 Hz, found results similar to those of Zhu et al.[3]

Nam et al.[6] applied vibration to the fluidization of Aerosil R974, increasing the bed expansion and reducing the minimum fluidization velocity. They estimated the fluidizing agglomerate size, density, external porosity, and terminal velocity by using a novel method that combined the fractal structure of the agglomerate and the Richardson-Zaki[7] equation, hereafter referred to as the R-Z equation. Nam et al.[6] also studied the mixing characteristics of the vibro-fluidized bed of nanoparticles by dying some of their nanosilica blue to act as a tracer. They found very good mixing after 2 min of fluidization (the entire column of particles turned blue) but concluded that the particles were mixed only on the microscale and not at nanoscale. A recent study of the effects of both mechanical and acoustic vibration on the fluidization of fumed silica Aerosil 200 was done by Levy et al.[8] By adding horizontal vibrations, they reduced the minimum fluidization velocity, which was further reduced by adding acoustic vibrations.

Zhu et al.[9] fluidized many different nanopowders conventionally, showing both APF and ABF type behavior. They took images of the fluidized agglomerates at the interface between the bed and the freeboard (in the splash zone) with a CCD camera and used image analysis software to find the average agglomerate size. They also estimated the average agglomerate size from initial and final bed height measurements combined with the R-Z equation, and obtained fairly good agreement with the measured values in the splash zone for APF type nanopowders. Recently, Wang et al.[10] measured the size of fluidized agglomerates of fumed silica Aerosil R974 in the splash zone by using a high resolution CCD camera and a planar laser sheet for illumination. Their experimental equipment and image analysis algorithm provided more accurate images of the fluidized nanoagglomerates than previous studies.

Yu et al.[11] used magnetic particles excited by an external oscillating magnetic field to enhance nanofluidization. However, in their experiments the magnetic particles were large (1–2 mm) and heavy (barium ferrite) and did not fluidize along with the nanopowder, but translated and rotated at the bottom of the column just above the gas distributor. The electromagnetic field was provided by coils located outside the column at the level of the distributor. They found that adding moving magnetic particles (excited by the magnetic field) enhanced the fluidization of nanoagglomerates quite significantly by breaking up clusters of agglomerates and by hindering the formation of bubbles. They were able to smoothly fluidize, without bubbles, large clusters (>500 μm) of Aerosil R974 nanopowder, and nanosize carbon black (Cabot Black Pearls 2000) pelletized to 800 μm by this method. These materials could not be fluidized at all with aeration alone. However, SEM images and EDX analysis showed that the mixing of two different species of nanopowders also occurs on the micron-scale and not on the nanoscale when using magnetically assisted nanofluidization.

Fumed silica, alumina, and titania nanoparticles have also been successfully fluidized in a rotating fluidized bed.[12,13] The centrifugal force acting on the agglomerates allowed fluidizing them at higher gas velocities without entrainment. A smooth surface and appreciable bed expansion were obtained when using APF nanopowders, but ABF nanopowders did not expand significantly due to bubbling. Nakamura and Watano[13] also studied mixing of different nanoparticles, nano-silica and nanoalumina in their rotating fluidized bed and found that mixing occurred at the microscale.

As an example of the potential applications of fluidization for dispersing nanoparticles, Hakim et al.[14] fluidized silica nanoparticles under reduced pressure conditions with vibration and coated them with alumina (a few nanometers thick) using atomic layer deposition (ALD). Even though the silica nanopowder fluidized as large agglomerates, each individual silica nanoparticle was found to be uniformly coated with alumina. This work shows the potential industrial application of using different nanoparticles as a catalyst support, where the catalyst can be evenly deposited on the surface of the nanoparticles by ALD or other coating methods in a fluidized bed.

Fluidization by jets

The effects of jets in fluidizing micron-sized particles have been widely studied and research in this field has been done with jets pointing upwards, downwards, or horizontally, and with nozzle sizes of the order of millimeters. These studies have shown that when properly designed, and at high gas velocities, jets enhance fluidization by promoting turbulent mixing. Research has focused on the gas and particle motion due to the jet, position and number of nozzles generating the jets, jet penetration length, jet expansion angles, and numerical simulations.[15–24] The hydrodynamic behavior of fine powders in jet-fluidized beds has also been studied,[25] and jet grinding or attrition of catalyst particles has been investigated both theoretically and experimentally,[26,27] showing the relationship between bed expansion and the generation of fines. A pertinent recent study describes the in situ fluidized bed jet grinding of carbon nanotubes during synthesis using a nozzle/target configuration placed above the distributor.[28]

In this article, a new method for enhancing the fluidization of agglomerates of nanoparticles is introduced. The method is based on the use of microjets produced by micronozzles

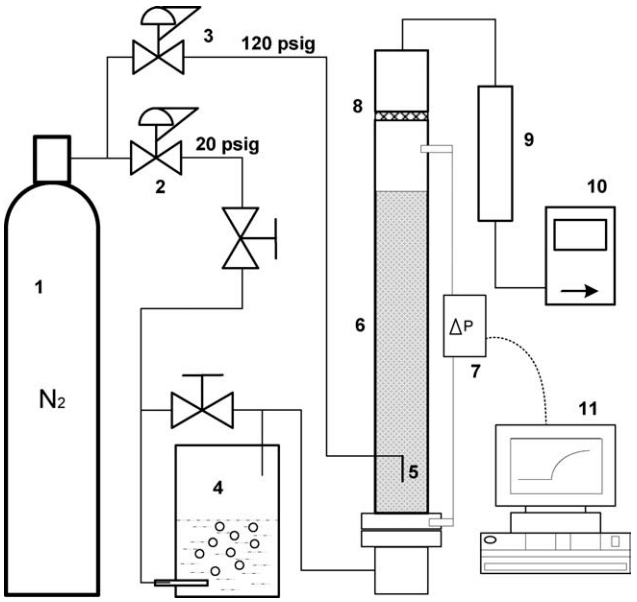

Figure 1. Schematic diagram of the experimental setup.

1: Compressed dry N_2 cylinder, 2: pressure regulator for low pressure, 3: pressure regulator for medium/high pressure, 4: tank for alcohol-water solution, 5: micronozzle, 6: fluidization column, 7: differential pressure transmitter, 8: pre-filter, 9: HEPA filter, 10: flowmeters, and 11: computer.

rather than millimeter sized nozzles (which were tried and found not to work), in the size range of 127–508 μm, pointing downwards at close distance to the air distributor. The use of microjets as a secondary flow, in addition to the flow through the distributor, produces very large bed expansions for APF type nanopowders. It also allows for the conversion of ABF into APF type behavior. As a result of applying the microjet(s), fluidized bed expansion of ABF nanopowders is increased several times, the fluidization is much smoother and more homogeneous, and the onset of bubbling is also delayed due to the better dispersion of the powder in the gas phase.

Experimental methods

Dry nitrogen was used as fluidizing gas supplied by a compressed cylinder with an initial pressure of around 2500 psig (17,225 kPa). Two-stage pressure regulators were used to produce a low pressure line at about 20 psig (137.8 kPa), and a medium pressure line at about 120 psig (826.8 kPa). The low pressure line feeds gas to the column through the distributor plate which is considered the primary flow. The medium pressure line supplies gas to the micronozzle or nozzles and is the secondary flow. Part of the primary flow is bubbled through a tank containing a dilute ethanol-water solution which substantially reduces electrostatic effects in the fluidized bed caused by triboelectrification.

Experimental set-up

A schematic diagram of the experimental setup is shown in Figure 1. The fluidization column is made of cast acrylic plastic and has an internal diameter of 3″ (7.62 cm) with a wall thickness of 0.25″ (0.635 cm). The height of the column can be changed from 5 feet (1.52 m) to 10 feet (3.05 m) by adding another tube on top of the main column. Pressure taps are located right above the distributor plate and just before the prefilter located at the top of the column. The taps are connected to three Cole-Parmer differential pressure transmitters with ranges from 0 to 0.5, 0 to 1, and 0 to 5″ of water (0 to 0.125, 0 to 0.25, and 0 to 1.25 kPa) connected to a Cole-Parmer digital display panel, and linked to a PC for data recording.

A sintered metal plate (Mott Corp.) located at the bottom of the column uniformly distributes the primary flow, the plate has 20 micron orifices with an open area of about 40% and a thickness of a few millimeters A woven mesh pre-filter with 20 micron apertures is placed at the top of the fluidization column. The gas flow then passes through a HEPA capsule (Pall Corp.) to remove any entrained small particles. Two Omega mass flow meters measure the flow exiting the column at ambient pressure so that a pressure correction factor is not needed for the flow. The flowmeters have ranges from 0 to 5 and from 0 to 20 l/min.

Nanopowders

The nanopowders used in these experiments were all supplied by Evonik Industries (formerly Degussa) and their properties are summarized in Table 1. It is important to note that APF and ABF type correspond to a classification based on fluidization behavior originally defined by Wang et al.[2] We have somewhat modified these two classifications as follows: agglomerate particulate fluidization behavior (APF) shows smooth, homogeneous fluidization similar to liquid fluidization, low U_{mf}, negligible elutriation of powder, large bed expansion (three to five times initial bed height or higher), minimal bubbling even at high gas velocities, and a well defined gas-particle interface; agglomerate bubbling fluidization (ABF) behavior exhibits channels, slugs, spouting, and is difficult to fluidize at low gas velocity, small bed expansion (less than two times initial bed height), high U_{mf}, large bubbles, substantial elutriation of powder, and a poorly defined gas-particle interface. Regarding the source of the

Table 1. Nanopowders Used and Their Properties

Brand	Type	Property	Fluidization Behavior	Source	Material	Primary Particle Size, (nm)	Surface Area, (m^2/g)	Tap Density, (kg/m^3)*
	R974	Hydrophobic	APF	comercial	SiO_2	12	170	50
Aerosil	200	Hydrophilic	APF	comercial	SiO_2	12	200	50
	90	Hydrophilic	ABF	comercial	SiO_2	20	90	80
	Raw 90	Hydrophilic	APF	process	SiO_2	20	90	80
Aeroxide	TiO_2 P25	Hydrophilic	ABF	comercial	TiO_2	21	50	130
	Alu C	Hydrophilic	ABF	comercial	Al_2O_3	13	100	50

*Primary particle size, density and surface area given by Degussa.

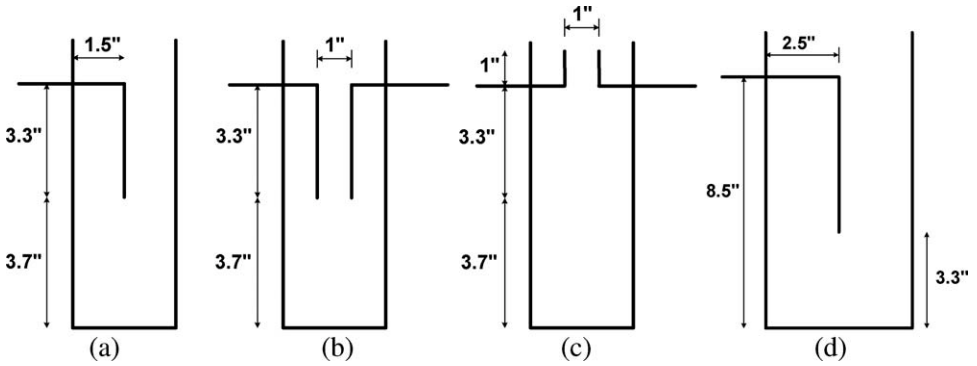

Figure 2. Detail of the locations of the nozzles inside the fluidization column, the bottom horizontal line is the gas distributor plate.

(a), (b), (c) correspond to the 3 in. (7.62 cm) ID column, and (d) corresponds to the larger scaled-up 5 in. (12.7 cm) ID column.

nanopowder, there are two types: commercial grade, powder delivered to customers which is usually compacted, and process or raw grade, where the nanopowder is taken directly from the process. Specific surface areas are measured by using the BET method and the tapped density is measured by applying vibration to a standard volume according to ISO787/11. In all the experiments reported in this work, the nanopowders were sieved to remove clusters of agglomerates larger than either 500 or 850 μm that are formed during transportation and storage.

Micronozzles

Micronozzles of different sizes 127, 177, 254, and 508 μm in diameter) welded to a 1/16″ ID (1.59 mm) copper tube were used in the experiments (Varian 1/16″ OD × 0.010″, 0.020″, 0.007″, 0.005″ ID × 5 cm SS) tube. Usually, the nozzle was pointing downwards at about 4″ (10.2 cm) from the distributor plate, since preliminary experiments showed better performance for the downward pointing nozzles. If one nozzle was used, it was located at the center of the column, and when using two or more nozzles, they were located symmetrically with about 1″ of separation between them. The nozzles were welded to copper tubing that connected them to the pressure regulator supplying the secondary flow at medium pressure. Figure 2 shows some of the different ways the nozzles were located in the fluidization column. Although a function of the size of the nozzle and nozzle pressure, the secondary flow entering through the nozzle(s) ranged from 10 to 40% of the total gas flow rate; however, other secondary flow rate ranges can also be used.

Internals

Several types of internals such as screens, sieve plates, or packing materials are commonly used in fluidization columns to enhance transport. Their purpose is usually to break-up bubbles in order to properly disperse the solid particles in the gas phase. They can also reduce axial mixing and change the particle residence time distribution, and if the product particles in a continuous fluidized bed have different physical properties than the feed particles, the internal can be used to concentrate the product in one section of the bed, for easier and more controllable discharge. However, some problems can arise due to the presence of internals, such as impeded solids motion and segregation of particles. Dead spots and channeling also occur if the powder is not homogeneously distributed on the internal structure.

To determine the effect of microjet assistance on the fluidization of nanoparticles in the presence of an internal, we conducted experiments using a wire mesh (Figure 3) to simulate a sieve tray as an internal in the fluidization column. The wire mesh had orifices of hexagonal shape; the thickness of the wire was of about 1.5 mm; and the dimensions of the openings were 4 × 8 mm^2. In these experiments, one downward pointing micronozzle (toward the internal) was used and located about 12″ (30.5 cm) above the distributor plate and about 4″ (10.2 cm) above the mesh. The nanopowder was fed from the top of the column and most of it was held by the mesh before the microjet flow was turned on.

Results and Discussion

The use of nondimensional variables is useful for purposes of comparison between experimental results. Nondimensional pressure drops are obtained by dividing the actual measured pressure drop by the apparent weight of the bed (weight of powder divided by cross-sectional area of the column). Similarly, the nondimensional bed height is obtained by dividing the actual bed height by the initial bed height of the bed of nanopowder at zero flow conditions when the powder has been just loaded into the fluidization column. Previous work in nanofluidization has shown that the nondimensional bed height or bed expansion is an excellent indicator of the quality of fluidization; the larger the bed expansion, the better the quality or smoothness of fluidization. Therefore we will compare the bed expansion for conventional and microjet-assisted nanofluidization and use the change in bed height as a metric for fluidization quality.

Hydrodynamic characteristics of conventional and microjet assisted fluidization of APF nanopowders

Aerosil R974 has been widely used in many nanofluidization articles reported in the literature because it fluidizes

Figure 3. Images showing the wire mesh grid used as an internal, (a) grid located 12 in. (30.5 cm) above the distributor, (b) micronozzle tip located 3.7 in. (9.40 cm) above the mesh.

[Color figure can be viewed in the online issue, which is available at www.interscience.wiley.com.]

readily showing APF type behavior; therefore, we have also used this nanopowder in our experiments using microjets for comparison with conventional fluidization. Three different amounts of Aerosil R974, 9.5, 13.3, and 20 g, were sieved to remove clusters of agglomerates greater than 850 μm and fluidized conventionally and with microjet assistance. Figure 4 shows the nondimensional bed expansion plotted against superficial gas velocity; it is important to note that the nondimensional bed heights are not dependant of the amount of fluidized powder.[29] The increase in bed height during jet processing for about 30 min at a constant gas velocity (squares) of about 2 cm/s is also shown in Figure 4. The resulting expansion of the bed when using the microjet as an assisting method is nothing short of remarkable. For example, during conventional fluidization at a gas velocity of 4 cm/s, the bed height expands about six-fold; however, when using microjet assistance, the bed height is about fifty times the initial bed height! Another characteristic observed during the experiments, and not clearly seen in the plot, is that the conventionally fluidized bed of Aerosil R974, although smooth and nonbubbling at gas velocities as high as six times the minimum fluidization velocity, starts to bubble at velocities greater than 3 cm/s. When microjet assistance is used, bubbling is not observed until 4.5 cm/s.

Figure 5 shows the plot of the nondimensional differential pressure drop across the fluidized bed during conventional and microjet assisted fluidization for the three different amounts of Aerosil R974. Note that the nondimensional pressure drops of the conventionally fluidized beds are always below one, indicating that not all the powder is being suspended by the gas. However, when microjet assistance is used, the nondimensional pressure drop is very close to one showing that almost the entire mass of powder is suspended by the gas flow. The minimum fluidization velocity (U_{mf}) is shown by the vertical lines at the points at which the pressure drop plateaus, and is about 0.5 cm/s for conventional fluidization and is reduced to about 0.25 cm/s when microjet assistance is used. In addition, at gas superficial velocities higher than 3 cm/s, the pressure drop starts to decrease for

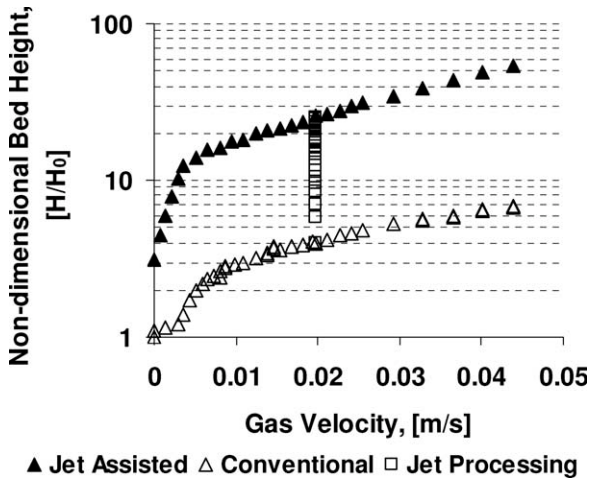

Figure 4. Comparison of the nondimensional fluidized bed height as a function of gas velocity for conventional and microjet assisted fluidization of Aerosil R974.

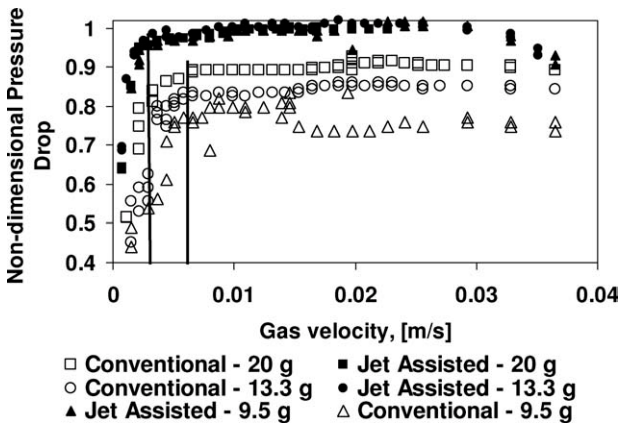

Figure 5. Nondimensional pressure drop as a function of gas velocity during fluidization of different amounts of Aerosil R974.

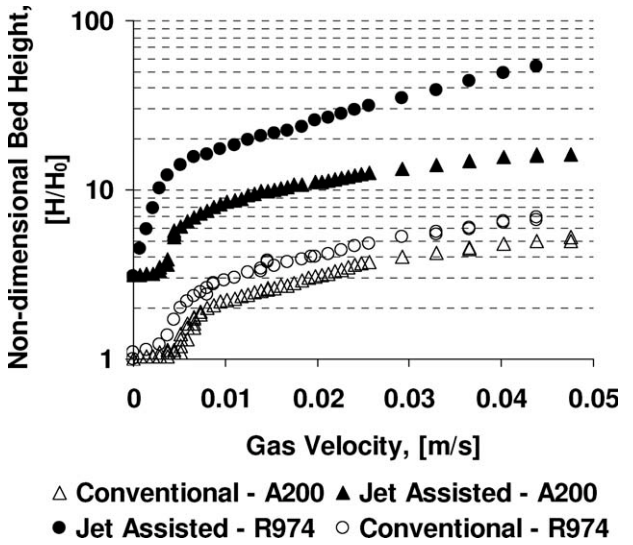

Figure 6. Comparison of the nondimensional bed height of Aerosil 200 and Aerosil R974.

the microjet assisted fluidization case; this may be due to the fact that there is a large bed expansion and more powder is in contact with the wall of the column; also, at these high velocities, some particle entrainment does occur which will lower the pressure drop.

Sieved Aerosil 200, the hydrophilic version of Aerosil R974, was also fluidized conventionally and with microjet assistance. Although Aerosil 200 expands much less in comparison with Aerosil R974 (see Figure 6), a much larger bed expansion is observed due to the microjet; for example, at a gas velocity of 4 cm/s the fluidized bed height of Aerosil 200 is about 11 times its initial bed height at no flow. During conventional fluidization, Aerosil 200 only expands up to 4.5 times its initial bed height. Another type of nanopowder that shows an APF behavior is "raw" Aerosil 90, which is a nanopowder that is directly extracted from the process, supplied to us by Degussa, and is not commercially available. This nanopowder was also sieved to remove clusters of agglomerates greater than 850 μm. Although not shown here, the behavior of raw Aerosil 90 is very similar to the behavior of Aerosil 200 with and without jet assistance.[29]

Hydrodynamic characteristics of conventional and microjet assisted fluidization of ABF nanopowders

As discussed in the Introduction, ABF nanopowders are characterized as being very difficult to fluidize, having a limited bed expansion, and rapidly developing bubbles making fluidization unstable and heterogeneous. Figure 7 shows the nondimensional bed expansion corresponding to the conventional fluidization of ABF nanopowders. The amounts and types of nanopowders used in these experiments are as follows: 18 grams of Aerosil 90, 22 grams of Aeroxide Alu C, and 60 grams of Aeroxide TiO_2 P25. These amounts of powder were chosen so as to keep the initial bed heights roughly the same. The nanopowders were sieved to remove agglomerates greater than 850 μm (Aeroxide Alu C and Aerosil 90) and agglomerates greater than 500 μm (Aeroxide TiO_2 P25).

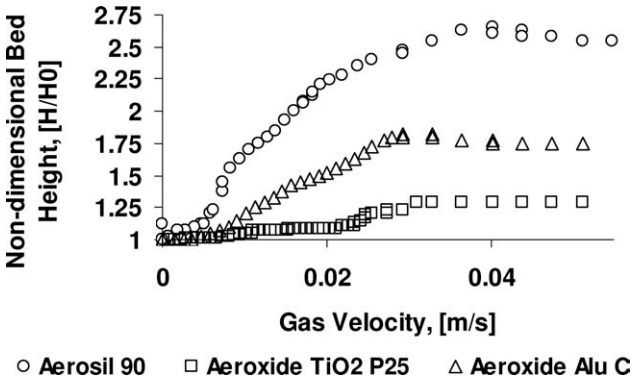

Figure 7. Nondimensional bed expansion as a function of gas velocity for conventional fluidization of ABF type nanopowders.

As seen in Figure 7, a maximum bed expansion of about 2.5 times the initial bed height is obtained for Aerosil 90, 1.75 for Aeroxide Alu C, and only 1.25 for Aeroxide TiO_2 P25. For these nanopowders, when the superficial gas velocity is increased above a certain value, i.e., the minimum bubbling velocity (U_{mb}), the bed does not expand further and the bed height remains constant. It is important to note that the Aerosil 90 nanopowder used in our experiments was relatively noncompacted and recently supplied by Degussa at the time of the experiments. Previous experiments by our group with Aerosil 90 that was stored for long periods of time resulted in a more difficult fluidization with expansions no more than 1.5 times the initial bed height (Zhu et al.[9]).

Figure 8 shows the fluidized bed heights as function of superficial gas velocity corresponding to microjet assisted fluidization of the three ABF nanopowders. It can be seen that Aerosil 90 and Aeroxide Alu C expand as much as 13–15 times their initial bed height and the bed expansion follows APF type behavior characterized by a linear increase in bed height with gas velocity (see for example, Figure 6). Aeroxide TiO_2 P25 expands up to 6.5 times its initial bed height,

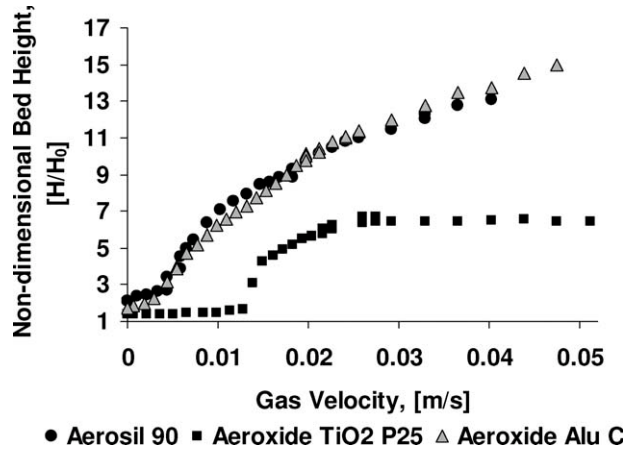

Figure 8. Nondimensional bed expansion as a function of gas velocity for microjet assisted fluidization of ABF nanopowders.

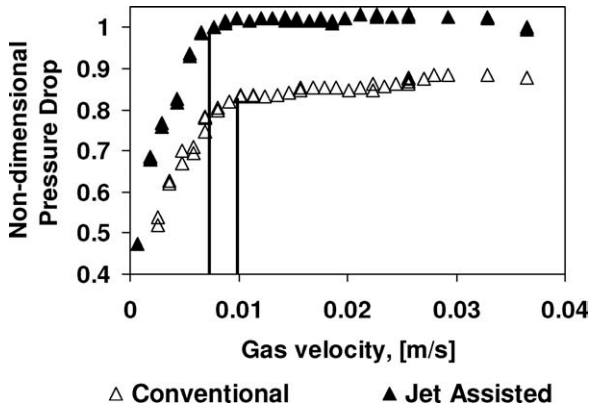

Figure 9. Nondimensional pressure drop as a function of gas velocity for fluidization of Aeroxide Alu C.

but the bed begins to bubble and the bed height remains constant at superficial gas velocities larger than 2.5 cm/s, which can be considered to be the minimum bubbling velocity (U_{mb}).

The corresponding nondimensional pressure drop plotted against superficial gas velocity is shown in Figure 9, for Aeroxide Alu C, with and without microjet assistance. Similar results, not shown here, were obtained for the other two ABF type nanopowders.[29] The figure shows that when microjet assistance is used, more powder is suspended in the gas phase since the pressure drop approaches the apparent weight of the powder (a nondimensional pressure drop equal to unity) and the minimum fluidization velocity, defined as the velocity where the pressure drop begins to plateau, is somewhat lower. Table 2 summarizes the hydrodynamic characteristics of all of the nanopowders, APF and ABF, used.

Effect of the micronozzle size on the microjet assisted fluidization

A set of experiments were done using the same type and amount (18 g) of commercial grade nanopowder, Aerosil 90, but with different nozzle sizes for the purpose of finding the optimal nozzle size for the microjet processing of the nanopowder. The micronozzles used had a diameter between 127 and 508 μm, and are listed in Table 3, along with their flow rates and axial exit velocities. The flow rates through the nozzles were measured by the flowmeters downstream of the fluidization column at ambient pressure and temperature. As the pressure upstream of all of the nozzles (except for the 508 μm nozzle) was kept at 120 psig (9.28×10^5 Pa absolute) and the upstream pressure of the 508 μm nozzle was varied between 20 and 120 psig (2.39×10^5 Pa absolute and 9.28×10^5 Pa absolute), the pressure at the nozzle will always be greater than the pressure of the surroundings (1.005×10^5 Pa absolute) into which the gas flow discharges, even when taking into account pressure losses in the tubing upstream of the nozzle. Therefore the flow through the micronozzles is said to be choked, sonic, or critical and the Mach number is equal to unity.[30,31] If we assume adiabatic, frictionless, compressible flow of nitrogen as a perfect gas through the nozzles, the temperature at the nozzle exit is 0.833 of the ambient temperature (298 K) or 248 K.[32] This results in a sonic velocity for nitrogen of about 320 m/s.

The bed of powder was conventionally fluidized at approximately 1.6 cm/s, then microjet assistance was started and the powder was processed for about 30–40 min until no further bed expansion was observed. Figure 10 shows the evolution of the nondimensional bed height as a function of the jet processing time. The bed heights level off after a certain time indicating that the agglomerates are not undergoing any further changes and that jet processing is close to completion. Two nozzles of about 127 μm (Red) and with an upstream pressure of 120 psig (9.28×10^5 Pa absolute) are slightly more effective than the rest of the tested nozzles. Among the single nozzles, a nozzle of about 254 μm (Blue) performs slightly faster than the others. A single 127 μm nozzle (Red) has the slowest performance. The performance is related to the amount of flow passing through the nozzle; a smaller nozzle diameter leads to smaller flow if the upstream pressure is kept constant. However, a smaller nozzle generates a higher shear and more turbulence (see Figure 12 later). By using two nozzles of 127 μm (Red), the flow through these two nozzles is less than the flow through a nozzle of 254 μm (Blue); however, as seen in Figure 10, they process the powder somewhat faster.

Figure 11 shows the nondimensional bed height as function of the superficial gas velocity of microjet processed Aerosil 90 (commercial grade). The figure shows that the size of the nozzle does not have a significant impact on the final bed expansion, but the largest bed expansion was obtained with the 254 μm (Blue) and the 127 μm (Red) nozzles. A slightly lower bed expansion was obtained with the 508 μm nozzle (Green). A larger nozzle diameter provides more gas flow, but

Table 2. Summary of the Hydrodynamic Characteristics of Conventional and Microjet-Assisted Fluidized Beds

			Conventional			Jet-Assisted			
Brand	Type	Mass (g)	ρb0 (kg/m^3)	Initial Bed Height H_0, (m)	Bed Height @ 3 cm/s H, (m)	ρb0 (kg/m 3)	Initial Bed Height H_0, (m)	Bed Height @ 3 cm/s H, (m)	Height Increase
	R974	9.45	40.8	0.051	0.279	13.2	0.157	1.763	531
	R974	13.3	38.3	0.076	0.411	13.4	0.218	2.451	496
Aerosil	200	15.7	29.5	0.117	0.470	9.4	0.366	1.560	232
	90	18.0	29.9	0.114	0.249	16.6	0.239	1.283	415
	Raw 90	21.2	17.8	0.260	0.889	16.6	0.279	1.524	71
Aeroxide	TiO2 P25	60	105.5	0.114	0.142	75.4	0.160	0.737	418
	Alu C	22	46.0	0.107	0.183	27.6	0.178	1.219	567

ρb0 corresponds to the bed density at zero fluidization flow.

Table 3. Micronozzles Used in the Experiments

Name	Size (μm)	Upstream Pressure (psig)	Flow (lpm)	Nozzle Velocity (m/s)
Red	127	120	0.4	320
Black	177	120	1.0	320
Blue	254	120	1.5	320
Green	508	20–120	*	320

*Flow rate varied depending on the upstream pressure.

the local shear rate, i.e., the change of the axial velocity as a function of radial position, is lower than for smaller nozzles. It is believed that the larger shear rate breaks-up the agglomerates more efficiently leading to larger bed expansion and better fluidization quality. Also, it was observed that for the 508 μm size nozzle, there was significant generation of electrostatic charge; this is believed to occur due to the large flow exiting the nozzle which produces electrostatic charge due to the excessive turbulence generated around the agglomerates. Hence, when using this nozzle, the upstream pressure was reduced to 20 psig (2.39×10^5 Pa absolute) to lower the flow rate through the nozzle.

To better understand the effect of the nozzle size on the microjet assisted fluidization results, it is of interest to visualize the velocity profile of the microjet generated by the flow exiting the micronozzle. For this purpose we consider only the gas phase without the solid phase, and if we also assume that the gas jet is round, the mean velocity profile is self-similar, and the turbulent viscosity is uniform, we can use available correlations in the literature[32] to plot the mean axial gas velocity profile as a function of radial and axial position. Figure 12 shows the mean axial velocity profiles as a function of radial position of two different micronozzles, 127 and 508 μm, and at an axial distance from the nozzle of 20 mm, and at upstream pressures of 120 psig (826.8 kPa) and 20 psig (137.8 kPa), respectively. The larger nozzle provides a higher flow than the smaller nozzle; however, the shear rate generated at the nozzle exit by the smaller nozzle is larger.

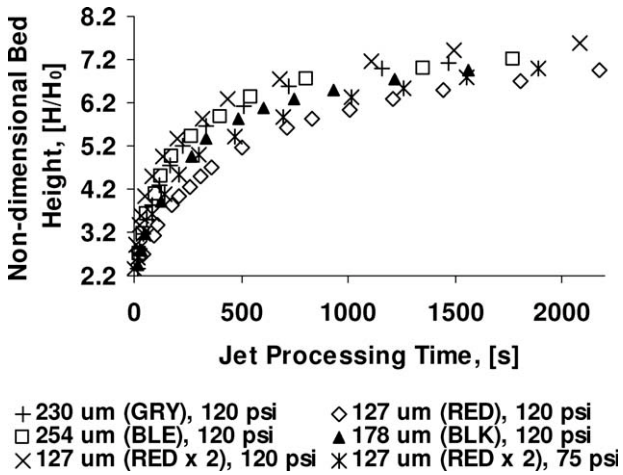

Figure 10. Nondimensional bed height during microjet processing of nanopowders as a function of processing time.

Gas velocity was held constant at about 1.6 cm/s.

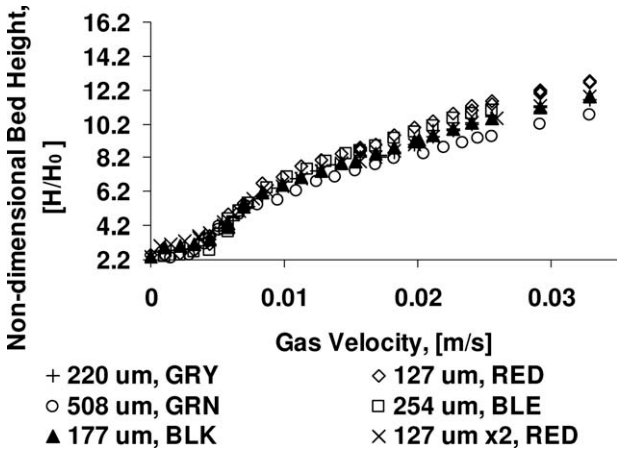

Figure 11. Nondimensional bed height as a function of gas velocity for microjet-assisted fluidization of Aerosil 90 using different nozzle sizes.

Effect of the direction of the micronozzle on fluidization of nanopowders

As explained earlier in the Experimental Methods section, all of the experimental results above were obtained by having the micronozzle or nozzles pointing downwards, and at a relatively short distance from the gas distributor plate, since this configuration gave the best results with regard to fluidization quality. However, the effect of having the nozzle(s) pointing upwards was also studied. Figure 13 compares the bed expansion of Aerosil 90 (commercial grade) for conventional and microjet assisted fluidization with the nozzle pointing in different vertical directions. The maximum bed expansion is obtained with the nozzle pointing downwards

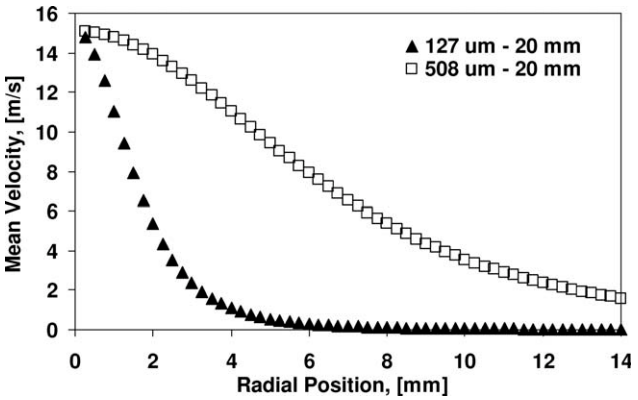

Figure 12. Theoretical velocity profile as a function of radial position 20 mm downstream of the nozzle tip for two different size nozzles (127 μm and 508 μm).

Because both operate at critical flow conditions, the velocities at the exit of the nozzle are the same even though the upstream pressure for the 127 μm nozzle is 120 psig (9.28×10^5 Pa absolute) while the upstream pressure for the 508 μm nozzle is 20 psig (2.39×10^5 Pa absolute). Both nozzles discharge to almost atmospheric pressure.

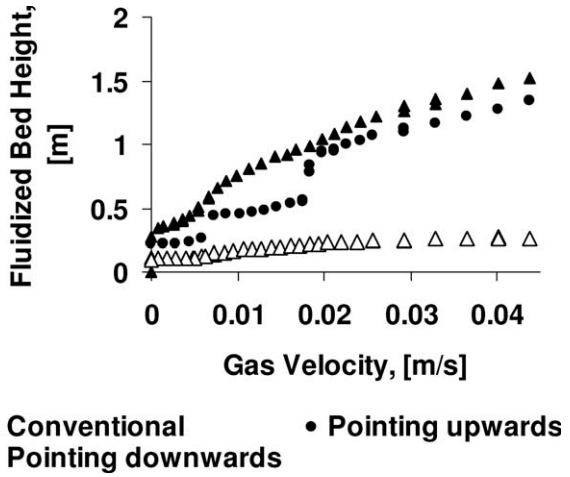

Figure 13. Effect of micronozzle direction on bed height for fluidization of Aerosil 90.

(dark triangles). When the jet is pointing upwards, the bed expansion is always lower than when the jet is pointing downwards, but is still appreciably higher than during conventional fluidization. It is important to note that only at high gas velocities are the bed heights for the two microjet assisted cases similar; below 2 cm/s, the bed collapses when the nozzle is pointing upwards. This means that the primary flow, i.e., the gas passing through the distributor plate, is very important and has to be relatively high in order to have fluidization in the section of the column below the level of the upward pointing nozzle.

Performance of an internal grid added to the fluidization column with and without microjet assistance

We have found that when fluidizing nanopowders, the use of microjets will allow taking full advantage of placing an internal in the fluidization column since the turbulent jet(s) will minimize the problems that arise due to its presence, i.e., impeded solids motion, segregation and nonhomogenous gas distribution. A wire mesh (see Figure 3) was placed about 12 in. from the air distributor plate and a micronozzle pointing downwards was located at about 4 in. above this mesh. Two series of experiments using process (raw) and commercial grades of Aerosil 90 were carried out with the wire mesh grid and microjet located as shown in Figure 3.

Figure 14 shows a comparison of the nondimensional bed heights when fluidizing raw Aerosil 90 corresponding to conventional fluidization, microjet assisted, and microjet assisted plus the wire mesh grid. This powder has an APF type behavior and expands readily during conventional fluidization, and if the powder is fully fluidized it passes easily through the grid. However, if the powder is sitting on the grid at the beginning of the experiment, the powder cannot be fluidized conventionally at any gas velocity due to poor distribution of gas by the grid and the formation of channels. The powder can only be fluidized with the jet acting on the grid.

Figure 15 shows images of the evolution of the raw Aerosil 90 powder bed from a packed bed condition to a fully fluidized bed by the action of the microjet on the internal grid, keeping the primary flow constant. Figure 15a shows the powder above the gas distributor plate beginning to fluidize due to the primary flow, but there is only a channel in the powder held by the grid; in Figure 15b, the microjet has been activated and pushes the nanopowder through the grid, and also aerates part of the powder held by the grid leading to a partially fluidized bed above the grid. In Figure 15c, d, more powder has passed through the grid and the volume below it is full with aerated powder that starts to move upwards and the entire bed expands, and in Figure 15e, a fully fluidized, homogeneous, expanded bed is seen.

When comparing the nondimensional bed heights of microjet assisted fluidization of commercial grade Aerosil 90 (ABF type behavior), with and without the presence of the mesh (not shown here), the fluidized bed heights are about the same at superficial gas velocities higher than 2 cm/s.[29] However, at gas velocities less than 2 cm/s, the bed height is lower when the grid is used because the gas velocity is not high enough to aerate the powder in the region above the gas distributor plate and below the grid. These results indicate that the impeded solids motion problem due to powder packing in a fluidized bed internal can be overcome for both APF and ABF type nanofluidization by applying the microjet.

Scale-up of the microjet assisted fluidization, experiments in a 5 in. (12.7 cm) internal diameter column

We have shown that microjets generated by micronozzles successfully enhance the fluidization of APF type nanopowders and can convert ABF type nanopowders into APF behavior. However, all the previous experiments were performed in a 3 in. (7.62 cm) internal diameter column and it is important to study how nanofluidization assisted by the microjets would behave in a larger diameter column, and,

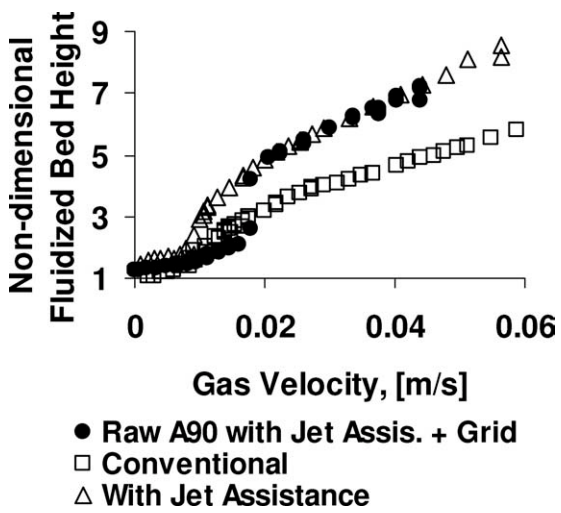

Figure 14. Effect of an internal (wire mesh grid) on the nondimensional bed height of raw Aerosil 90 (process grade) fluidized with microjet assistance.

Conventional fluidization data without the grid are shown as a comparison.

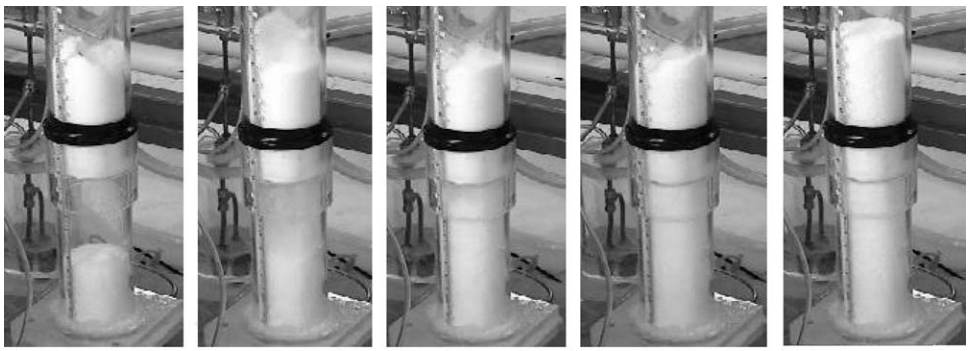

Figure 15. Images showing the evolution of the fluidized bed of raw Aerosil 90 nanopowder with an internal grid assisted by a microjet.

Primary flow passing through the distributor is kept constant. (a) primary flow only, no nozzle flow, most of the powder sitting on the grid, (b) jet has been activated and acts on the grid, powder starts to pass through, (c) fluidization starts, (d) section below the grid is filled with fluidized powder that easily passes through the grid, (e) the entire bed of powder is fluidized, a condition promoted by the jet.

for example, how many jets would be necessary to obtain an enhanced fluidization in a pilot or plant scale column? Small diameter columns have large wall effects, and for ABF type nanopowders, bubbles can occupy the entire cross-sectional area at certain gas velocities. Therefore, a fluidization column diameter of 5 in. (12.7 cm) was selected to reduce wall effects and to verify that the microjet assisted method would also work well in a larger diameter column.

We chose Aeroxide TiO2 P25 to be studied in the larger lab scale column because this nanopowder shows typical ABF type behavior and is one of the most difficult to fluidize, yet it can be used in many industrial applications due to its excellent catalytic and photosensitive properties. Figure 16 shows a comparison of the nondimensional fluidized bed heights of conventional and microjet assisted fluidized beds of Aeroxide TiO2 P25 using 2 different sized micronozzles, 254 μm at 75 and 120 psig (516.8 and 826.8 kPa) and 508 μm at 20 psig (137.8 kPa). Similarly to what we observed in the 3 in. diameter column, during conventional fluidization the bed bubbles vigorously and hardly shows any expansion, but when microjet assisted, the nanopowder could be fluidized at 2.5 cm/s without bubbles and expands about five times its initial bed height. The effect of the different size micronozzles and pressures are small, with the highest bed expansion observed for the 254 μm nozzle at 75 psig (516.8 kPa). Figure 17a shows the initial bed height of Aeroxide TiO2 P25 in the 5 in. column at zero gas velocity, Figure 17b shows a view of the same amount of nanopowder fluidized with microjet assistance expanded to 25.5 in. (64.8 cm), and Figure 17c shows a close-up of the clearly defined fluidized bed surface without any bubbles.

Mixing and blending two nanopowders using microjet assistance

As discussed in the Introduction section, previous researchers, Nam et al.,[6] Yu et al.,[11] and Nakamura and Watano[13] examined the effects of vibration, moving magnetic particles excited by an oscillating magnetic field, and using a centrifugal field in a rotating bed on the mixing and blending of different species of nanopowders. All of these researchers found that nanofluidization assisted by these external fields quickly mixed the nanopowders, but when examined under SEM and EDX they were found to mix on the microscale rather than on the nanoscale. As microjet processing will cause the nanofluidized bed to expand much more than these other methods, we also studied the degree of mixing of two different nanopowders.

Iron-oxide (primary particle size, 3 nm) and Aeroxide Alu C alumina (primary particle size, 13 nm) were fluidized with and without jet processing for about 30 min or until no further bed expansion was observed. The ratio of the weight of iron-oxide to alumina was 1/10. Figure 18 show different stages during mixing of these nanopowders using the microjet assisting method. Highlights of the process include the change in fluidization behavior from an initial ABF type to an APF type behavior as seen by the bed expansion, and the change in color of the mixed nanopowder. At the very

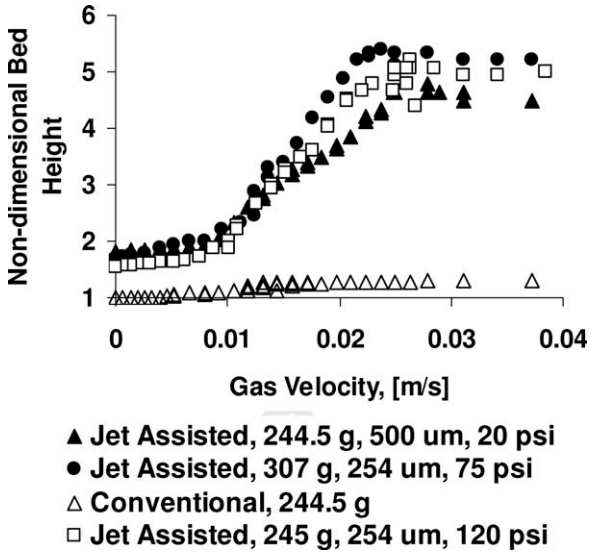

Figure 16. Nondimensional bed height for fluidization of Aeroxide TiO_2 P25 in a 5 in. (12.7 cm) ID column.

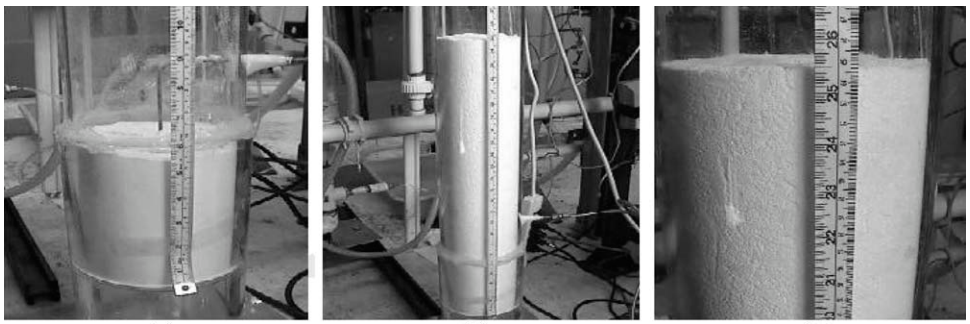

Figure 17. Images corresponding to the fluidization of Aeroxide TiO_2 P25 in a 5 in. (12.7 cm) ID column.

(a) Initial bed height, (b) maximum bed height when fluidized with microjet assistance, (c) close-up of the fluidized bed surface, bed expanded from 5.5 (14.0 cm) to 25.5 in. (64.8 cm) and surface of the bed shows no bubbles.

beginning, the bed has a dark brown color typical of the iron oxide (alumina is white), but after microjet processing the color has been downgraded to an orange tone rather than the light brown color observed when mixing at the microscale using vibration or magnetic assistance.

A small quantity of the two powder samples were then placed on carbon grids and looked at under TEM-EELS. Figure 19 shows images of the powder samples: (a) conventional fluidization, and (b) with microjet processing. As the electron beam was moved along the powder area of the jet processed sample, Figure 19b, an iron peak in the EELS spectrum (Figure 19c) appeared or disappeared depending on whether iron was present or not, indicating a well-mixed sample of iron oxide and alumina on the nanoscale (note the 20 nm scale bar). No iron peak was observed on the sample fluidized without microjet processing indicating that it was all alumina. Different areas of these two samples examined under TEM-EELS showed similar characteristics, i.e., good mixing on the nanoscale using microjet assistance,

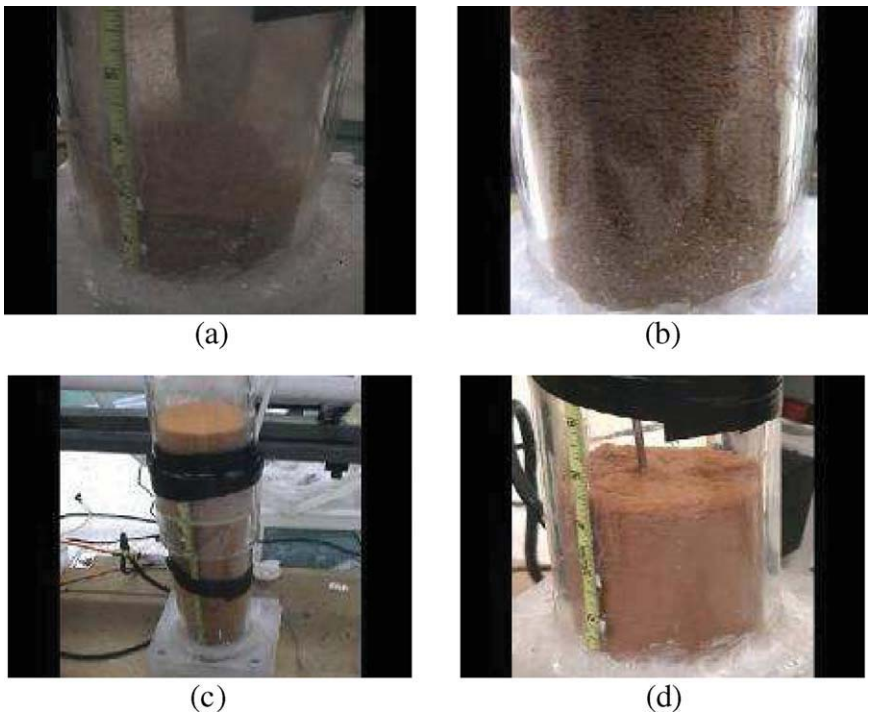

Figure 18. Jet assisted mixing of 2 different nanopowders: alumina (white) and iron oxide (dark brown).

(a) Start of the experiment using aeration alone, bed height is less than 3 in. (7.62 cm), tip of the downward nozzle can be seen at 5 in (12.7 cm) above the distributor. The dark brown color of the iron oxide is predominant. (b) Although microjet processing, the bed has expanded and there are white agglomerates at the bottom of the bed. (c) At the end of mixing, the bed height is several times the initial bed height and fluidization behavior changed from ABF to APF. (d) Bed of mixed powder without any fluidizing gas, final bed height is about 4.5 in. (11.4 cm), almost double the initial bed height indicating a change in bulk density. The bed has a different color indicating that mixing on the nanoscale may have occurred.

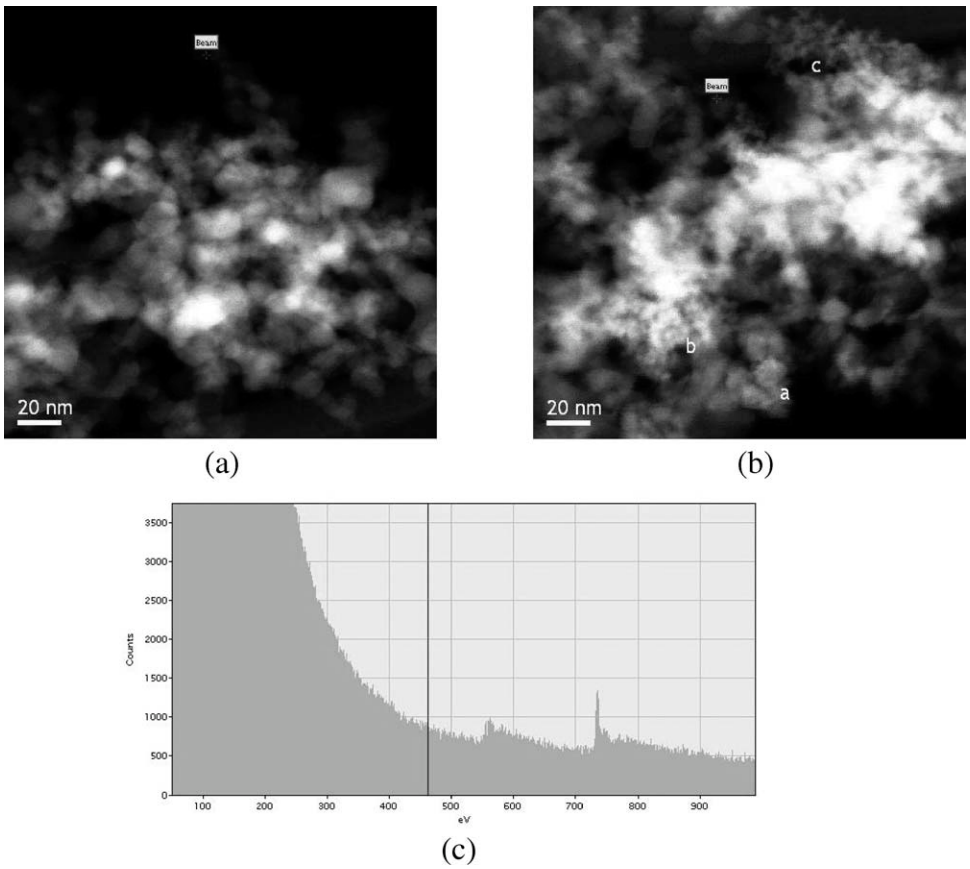

Figure 19. TEM-EELS measurements of iron oxide (primary particle size, 3 nm) and alumina (primary particle size, 13 nm) mixed samples on a carbon grid.

As the electron beam was moved along the powder area, the iron peak appeared or disappeared depending on whether iron was present or not. (a) Conventional fluidization, no iron peaks observed anywhere indicating only alumina. (b) All of the imaged area showed iron and alumina present throughout, e.g., points a, b, c, indicating a well-mixed sample on the nanoscale. (c) Spectrum, iron peak at about 730 ev seen throughout sample (b) but not in sample (a).

and at best, microscale mixing during conventional fluidization.

Concluding Remarks

We have shown that by using a microjet generated by a micronozzle, APF type behavior nanopowders will expand several times more, relative to the already expanded conventional fluidized bed height, and show smooth fluidization without bubbling even at high gas velocities. For example, Aerosil R974 will expand up to 50 times its original bed height after being subjected to microjet processing. For nanopowders that normally show ABF type behavior such as Aeroxide TiO2 P25, microjet assistance will transform their fluidization behavior into APF type characterized by the absence of bubbles and a fluidized bed expansion several times the initial bed height. We have also found that the best performance was achieved by positioning the nozzle relatively close to the gas distributor plate at the bottom of the column and pointing downwards. Micronozzles pointing upwards will also work, but there is some powder between the distributor and the nozzles that may not participate in the fluidization.

Experiments were conducted with nozzles of different sizes (from 127 up to 508 μm) and at an upstream pressure of 20–120 psig (516.8 and 826.8 kPa). The smaller the nozzle size the higher the shear generated by the jet, but also the lower the gas flow passing through the orifice of the nozzle. For example, for many nanopowders we found that the optimal nozzle sizes were between 127 and 254 μm. These nozzle sizes provided a jet with enough shear and sufficient gas velocity to result in generating turbulence and breaking of large nanoagglomerates. However, some ABF nanopowders, such as Aeroxide TiO2 P25, only require high turbulence for achieving an APF behavior. For these nanopowders a larger nozzle size was used (508 μm) but with a lower upstream pressure (20 psig) since extremely high jet flow rates are not desirable because they generate electrostatic charge which can cause the nanopowder to stick to the wall of the column and the bed to defluidize.

The rate at which the agglomerates were processed by the jet was also studied and it was found that this depends on the total superficial gas velocity, the size and number of the nozzles, and the upstream nozzle pressure. A microjet processing time of about 20–30 minutes is usually sufficient to obtain a maximum bed expansion. As the main purpose of enhancing the fluidization of these nanopowders was for

industrial applications, scale up of the microjet assisted system was also studied. It was demonstrated that the jet assisted fluidization also gives good results in a larger 5″ (12.7 cm) diameter column. Also, adding microjets in a fluidized bed of nanopowder equipped with an internal grid to simulate a sieve tray will generate turbulence, high shear, and good mixing, and allow the powder to pass through the grid towards the bottom of the bed for easy removal from the fluidized bed.

Although few experiments were performed using iron-oxide and alumina nanopowders, it appears that microjet assisted gas-fluidization, can mix and blend two different nanopowders at the nanoscale. This was not achieved when mixing nanopowders in a fluidized bed using either vibration, moving magnetic particles, or a centrifugal field as the assisting method.

Acknowledgments

The authors would like to acknowledge support from the National Science Foundation through Grant # DMI 0210400, NIRT-Collaborative Research: Experimental and Computational Investigations of Fluid Interactions/Transport in Nanodomains and Around Nano-particles. Financial and technical support from Evonik Industries (formerly Degussa), and in particular, from Drs. Herbert Riemenschneider and Jonah Klein are also gratefully acknowledged. The authors also would like to thank Dr. Peter Crozier of ASU for making the TEM-EELS measurements.

Literature Cited

1. Geldart D. Types of gas fluidization. *Powder Technol*. 1973;7:285–292.
2. Wang Y, Gu G, Wei F, Wu J. Fluidization and agglomerate structure of SiO_2 nanoparticles. *Powder Technol*. 2002;124:152–159.
3. Zhu C, Liu G, Yu Q, Pfeffer R, Dave R, Nam C. Sound assisted fluidization of nanoparticle agglomerates. *Powder Technol*. 2004;141:119–123.
4. Guo Q, Liu H, Shen W, Yan X, Jia R. Influence of sound wave characteristics on fluidization behaviors of ultrafine particles. *Chem Eng J*. 2006;119:1–9.
5. Guo Q, Li Y, Wang M, Shen W, Yang C. Fluidization characteristics of SiO2 nanoparticles in an acoustic fluidized bed. *Chem Eng Technol*. 2006;29:78–86.
6. Nam C, Pfeffer R, Dave R, Sundaresan S. Aerated vibrofluidization of silica nanoparticles. *AIChE J*. 2004;50:1776–1785.
7. Richardson JF, Zaki WN. Sedimentation and fluidization. Part I *Trans Instn Chem Engrs*. 1954;32:35–53.
8. Levy E, Celeste B. Combined effects of mechanical and acoustic vibrations on fluidization of cohesive powders. *Powder Technol*. 2006;163:41–50.
9. Zhu C, Yu Q, Pfeffer R, Dave R. Gas fluidization characteristics of nanoparticle agglomerates. *AIChE J*. 2005;51–2:426–439.
10. Wang XS, Palero V, Soria J, Rhodes MJ. Laser-based planar imaging of nano-particle fluidization: Part I - determination of aggregate size and shape. *Chem Eng Sci*. 2006;61:5476–5486.
11. Yu Q, Dave R, Zhu C, Quevedo J, Pfeffer R. Enhanced fluidization of nanoparticles in an oscillating magnetic field. *AIChE J*. 2005;51:1971–1979.
12. Quevedo JA, Pfeffer R, Shen Y. Dave RN, Nakamura H, Watano S. Fluidization of nanoagglomerates in a rotating fluidized bed. *AIChE J*. 2006;52:2401–2412.
13. Nakamura H, Watano S. Fundamental particle fluidization behavior and handling of nano-particles in a rotating fluidized bed. *Powder Technol*. 2008;183:324–332.
14. Hakim LF, Blackson J, George SM, Weimer AW. Nanocoating individual silica nanoparticles by atomic layer deposition in a fluidized bed reactor chem vapor deposition. 2005;11:420–425.
15. Clift R, Filla M, Massimilla L. Gas and particle motion in jets in fluidized beds. *Int J Multiphase Flow*. 1976;2:549–561.
16. Blake TR, Webb H, Sunderland PB. The non-dimensionalization of equations describing fluidization with application to the correlation of jet penetration height. *Chem Eng Sci*. 1990;45:365–371.
17. Hong RY, Li H, Wang Y. Studies on the inclined jet penetration length in a gas-solid fluidized bed. *Powder Technol*. 1997;92:205–212.
18. Hong RY, Li HZ, Cheng MY, Zhang JY. Numerical simulation and verification of gas-solid jet fluidized bed. *Powder Technol*. 1996;87:73–81.
19. Hong RY, Guo QJ, Luo GH, Zhang JY, Ding J. On the jet penetration height in fluidized beds wit two vertical jets. *Powder Technol*. 2003;133:216–227.
20. Zhong W, Zhang M. Jet penetration depth in a two-dimensional spout-fluid bed. *Chem Eng Sci*. 2005;60:315–327.
21. Chyang CS, Chang CH, Chang JH. Gas discharge modes at a single horizontal nozzle in a two-dimensional fluidized bed. *Powder Technol*. 1997;90:71–77.
22. Vaccaro S. Analysis of the variables controlling gas jet expansion angles in fluidized beds. *Powder Technol*. 1997;92:213–222.
23. Yang WC. Comparison of jetting phenomena in 30-cm and 3-m diameter semicircular fluidized beds. *Powder Technol*. 1998;100:147–160.
24. Guo Q, Yue G, Zhang J, Liu Z. Hydrodynamic characteristic of a two-dimensional jetting fluidized bed with binary mixtures. *Chem Eng Sci*. 2001;56:4685–4694.
25. Hong R, Ding J, Li H. Fluidization of fine powders in fluidized beds with an upward or a downward air jet. *China Particuol*. 2005;3:181–186.
26. Wether J, Xi W. Jet attrition of catalyst particles in gas fluidized beds. *Powder Technol*. 1993;76:39–46.
27. Tasirin SM, Geldart D. Experimental investigation on fluidized bed jet grinding. *Powder Technol*. 1999;105:337–341.
28. Baddour CE, Briens CL, Bordere S, Anglerot D, Gaillard P. The fluidized bed grinding of carbon nanotubes with a nozzle/target configuration, *Powder Technol*. 2009;190:372–384.
29. Quevedo JA. Fluidization of Agglomerates of Nanoparticles Under Different Force Fields, PhD Thesis, New Jersey Institute of Technology, 2006.
30. Tilton JN, Sakiadis BC. *Section 6: Fluid and Particle Dynamics. Perry's Chemical Engineering Handbook*, 7th ed. New York, NY: McGraw-Hill, 1997.
31. Ward-Smith AJ. Critical flowmetering: the characteristics of cylindrical nozzles with sharp upstream edges. *Int J Heat Fluid Flow*. 1979;1:123–132.
32. Pope SB.*Turbulent Flows: Free Shear Flows*.Cambridge, UK: Cambridge University Press, 2000.

Manuscript received May 31, 2009, and revision received Aug. 10, 2009.